

Correlating 3D Surface Atomic Structure and Catalytic Activities of Pt Nanocrystals

Sungin Kim, Jimin Kwag, Chiara Machello, Sungsu Kang, Junyoung Heo, Cyril F. Reboul, Dohun Kang, Seulki Kang, Sangdeok Shim, So-Jung Park, Byung Hyo Kim, Taeghwan Hyeon, Peter Ercius,* Hans Elmlund,* and Jungwon Park*

Cite This: *Nano Lett.* 2021, 21, 1175–1183

Read Online

ACCESS |

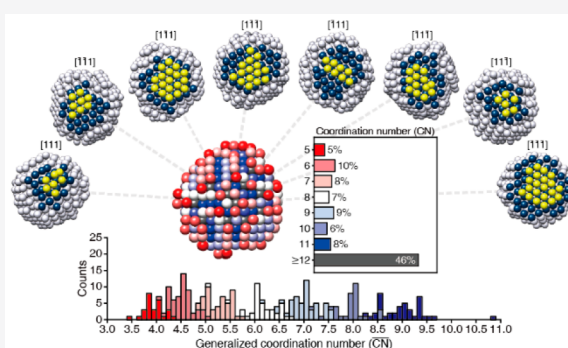
Metrics & More

Article Recommendations

Supporting Information

ABSTRACT: Active sites and catalytic activity of heterogeneous catalysts is determined by their surface atomic structures. However, probing the surface structure at an atomic resolution is difficult, especially for solution ensembles of catalytic nanocrystals, which consist of heterogeneous particles with irregular shapes and surfaces. Here, we constructed 3D maps of the coordination number (CN) and generalized CN (\overline{CN}) for individual surface atoms of sub-3 nm Pt nanocrystals. Our results reveal that the synthesized Pt nanocrystals are enclosed by islands of atoms with nonuniform shapes that lead to complex surface structures, including a high ratio of low-coordination surface atoms, reduced domain size of low-index facets, and various types of exposed high-index facets. 3D maps of \overline{CN} are directly correlated to catalytic activities assigned to individual surface atoms with distinct local coordination structures, which explains the origin of high catalytic performance of small Pt nanocrystals in important reactions such as oxygen reduction reactions and CO electro-oxidation.

KEYWORDS: Surface atomic structure, 3D coordination map, 3D atomic structure, Surface coordination number, Structure-catalytic activity relationship, Nanocrystal imaging



The chemical activity of heterogeneous catalysts is predominantly determined by their surface structures, which is explained by the fact that chemical reactions and adsorption properties of molecular species are regulated by atomic surface geometries.^{1–14} Heterogeneous catalysts composed of a single or a few kinds of facets are commonly synthesized in order to efficiently exploit such surface sensitivity in catalytic reactions. Metal nanocrystals with cubic, octahedral, and cuboctahedral shapes selectively enclosed by {111} and {100} facets are good examples that show superior activity or selectivity for many important catalytic reactions.^{15–24} These nanocrystals have well-defined surface structures that allow mechanistic understanding of surface reactions based on bulk surface chemistry and theoretical calculations. However, heterogeneous catalysts with controlled facets are of limited practical use due to the difficulties in creating homogeneous synthetic thermodynamics and surface structure geometries in batch-scale synthesis.^{24–26}

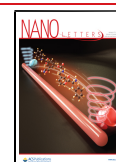
Conventional heterogeneous catalysts with broader industrial applications, such as small (<3 nm in diameter) Pt nanocrystals, are generally heterogeneous in size, shape, and surface atomic structures.^{27,28} It is desirable to reduce the size of the nanocrystal catalysts as a route to maximize the surface area and reduce material costs. Small nanocrystals have a more complicated

surface structure with a large fraction of edge and corner atoms.^{29–33} Thus, it becomes difficult to interpret the complex surface structures to identify active sites and understand their contributions to the catalytic activity. Methods have been developed to interrogate the surface atomic structures of individual heterogeneous catalysts. Combining two-dimensional (2D) imaging with Cs-corrected high-resolution transmission electron microscopy (HR-TEM) and exit wave restoration showed that the low-index facets of Pt nanocrystals on a carbon support are not flat.^{34,35} However, these results only show a projected 2D view of the three-dimensional (3D) surface. More recently, scanning-TEM (STEM) tomography, where the 3D atomic structure is reconstructed from a tilt series of 2D STEM projections, was applied to catalytic nanocrystals in a vacuum.^{36–39} This method has successfully resolved 3D atomic structures of catalysts with sizes above 7 nm.^{36–39}

Received: December 11, 2020

Revised: January 4, 2021

Published: January 8, 2021



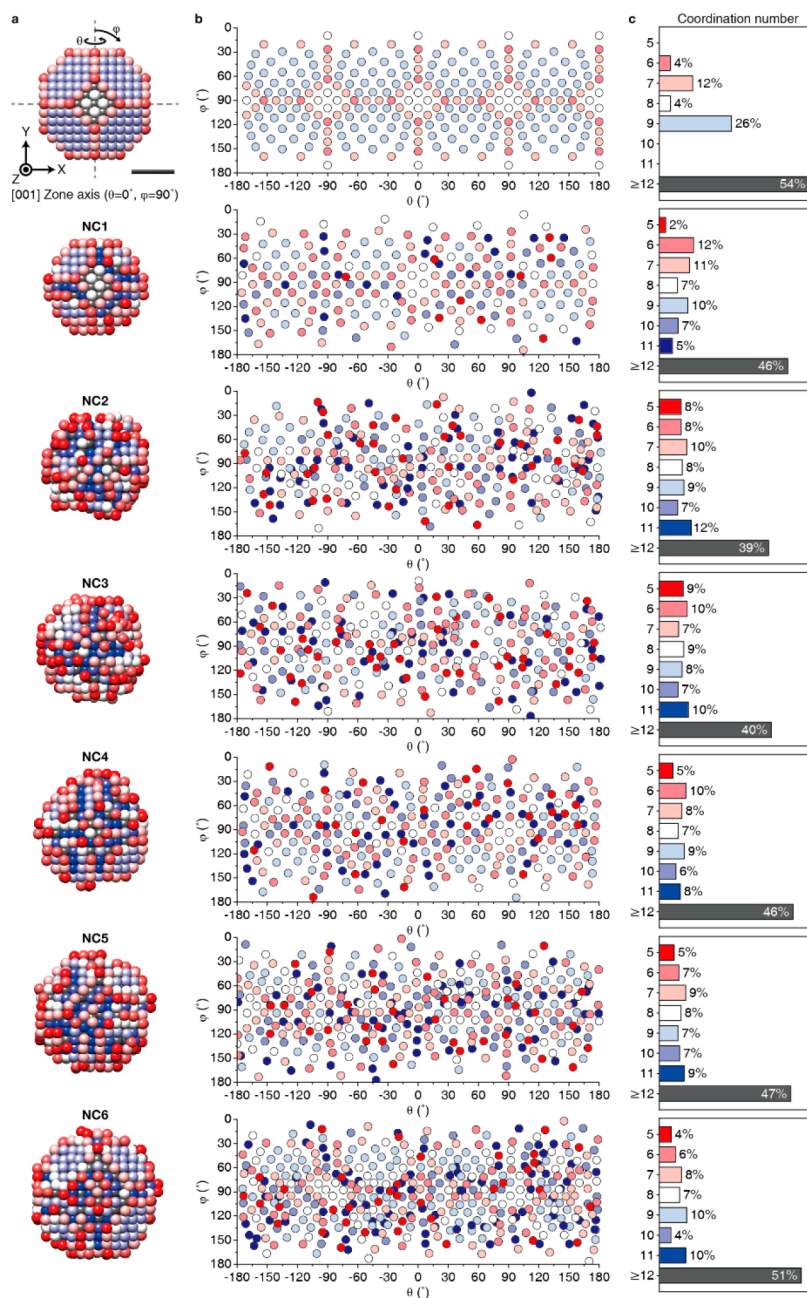


Figure 1. 3D mapping CNs of constituent atoms in Pt nanocrystals. (a) 3D atomic structures of the truncated octahedral fcc model and six synthesized Pt nanocrystals. All of the constituent atoms in the 3D maps are colored by CNs. Scale bar, 1 nm. (b) 2D color maps in the spherical coordinate of surface atoms. Cartesian coordinates of surface atoms are converted into the 2D plane in spherical coordinates with radial normalization. (c) Histograms for the portion of CNs in all constituent atoms. In contrast to the fcc model structure, synthesized Pt nanocrystals have surface atoms with CN = 10–11.

Recently, a new method, “one-particle 3D reconstruction”, for determining the 3D atomic structures of nanocrystals in solution has been developed.⁴⁰ Using 3D atomic structures of sub-3 nm sized Pt nanocrystals derived from this method,⁴⁰ we here introduce a quantitative method that connects the surface structures to the catalytic activities of heterogeneous catalysts in an atom-by-atom manner. Coordination number (CN) and generalized CN (\overline{CN}) for all constituent atoms are measured and displayed in the 3D structures of individual Pt nanocrystals. The obtained distribution of surface atoms reveals that sub-3 nm sized Pt nanocrystals are enclosed by islands of atoms with irregular shapes at the solid/liquid interface. This leads to

nonuniform surface structures that are directly linked to the catalytic activity of the nanocrystals. Obtained 3D maps are correlated to overpotential for the important fuel cell catalytic reactions, oxygen reduction reaction (ORR), and CO electro-oxidation, assigned for individual surface atoms. Our results provide the structural origin of the high performance for small Pt nanocrystals for various catalytic reactions.

RESULTS AND DISCUSSION

The understanding of the electronic structures and the establishment of structure–function relationships for Pt nanocrystals have been based primarily on the assumed face-centered

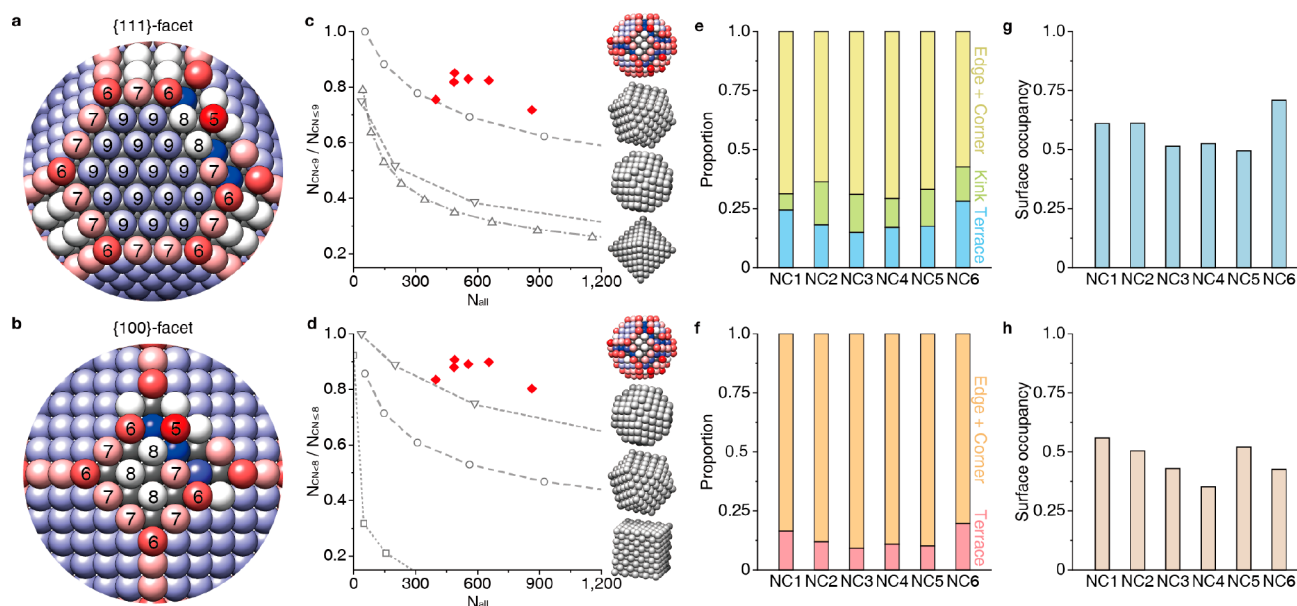


Figure 2. Quantitative analysis of surface atoms of synthesized Pt nanocrystals. (a, c, e, g) Surface structure analysis for {111} facets. (b, d, f, h) Surface structure analysis for {100} facets. (a, b) Visual aids for types of surface atoms and corresponding CNs along (a) {111} and (b) {100} facets. (c, d) Ratio of low-coordination surface atoms for six synthesized Pt nanocrystals and various sized fcc model structures along (c) {111} and (d) {100} facets. Red diamonds indicate synthesized Pt nanocrystals. Gray circles, gray reverse triangles, and gray squares indicate cuboctahedral, truncated octahedral, octahedral, and cubic fcc model structures, respectively. (e, f) Structural composition of surface atoms on six synthesized Pt nanocrystals along (e) {111} and (f) {100} facets. Yellow, green, and blue bars mean edge or corner, kink, and terrace atoms in {111} facets, respectively. Orange and red bars indicate edge or corner and terrace atoms in {100} facets, respectively. (g, h) Averaged surface occupancy for (g) {111} and (h) {100} facets for individual Pt nanocrystals.

cubic (fcc) atomic arrangement of the bulk material. In such an ideal monatomic fcc structure, atoms with full coordination of nearest neighbors have a CN = 12. The CN of surface atoms reduces from 12, depending on the geometry of the surface facet exposed (Figure 1, top row). The atomic surface geometries in terms of CN are related to the chemical bond formation and catalytic activity confined to the surface.^{41–44} We here analyzed the surface structures and CNs of the atoms of sub-3 nm synthesized Pt nanocrystals based on our previously published 3D density maps reconstructed with 3D SINGLE (Structure Identification of Nanoparticles by Graphene Liquid cell Electron microscopy).⁴⁰ The reconstructed 3D density maps have a resolution better than 1 Å, which allows the assignment of the positions (X-Y-Z) of the constituent atoms with a precision of ± 19 pm. The obtained 3D atomic coordinates show that the core of the synthesized nanocrystals is generally crystalline with a face-centered cubic structure, but there are marginal deviations from the expected bulk structure near the surface, resulting in highly nonuniform surface structures that have not been previously characterized in detail.

We present the CN of all constituent atoms of six synthesized Pt nanocrystals in Figure 1. Each Pt nanocrystal, named consecutively from NC1 to NC6, has a diameter of 2.25, 2.41, 2.42, 2.52, 2.66, and 2.92 nm, respectively (Figure 1a, Figure S1, and see Methods in Supporting Information). The surface atoms are visualized in 3D, colored according to CN (Figure 1a), on a 2D plane in spherical coordinates with radial normalization according to their angular position at the surface (Figure 1b) and in 2D sliced planes of the fcc crystal axes (Figure S2). Compared to the ideal fcc model structure (Figure 1, top row), CNs for surface atoms in the NCs are diverse, and their positions in the angular distribution maps are less regular. The distribution of CNs for all constituent atoms in the fcc model and the six Pt

nanocrystals is shown as histograms (Figure 1c). Notably, the experimentally derived Pt nanocrystal structures have a significant portion of atoms with CN = 10–11, whereas these are absent in the fcc model structures (Figure 1c and Figure S3). The atoms with CN = 10–11 are missing one or two coordinating atoms and are, therefore, positioned below vacant sites on terraces or along edges of the surface (Figure S4). The vacancies on the terrace are thermodynamically less stable than those on the edge. This implies that atoms with CN = 10–11 are more likely to be below edges along monatomic step structures (Figure S4). When the surface atoms on edges were removed, atoms with CN = 10–11 appear, and the portion of edge and corner increases, while the portion of terrace decreases (Figure S5).

Nanocrystals with fcc structures are expected to form morphologies mainly truncated by {111} and {100} facets according to traditional Wolff constructions and surface energies. These are thermodynamically stable because they have high atomic coordination numbers. The surfaces of the sub-3 nm Pt nanocrystal structures analyzed here can be understood based on surface truncation by highly coordinated terraces of {111} and {100} and less-coordinated arrangements such as an edge, corner, kink, and step. Atoms located in different local structures have specific CN on different low-index facets, allowing us to determine the type of atom from its CN. On {111} facets, a CN = 9, 8, and ≤ 7 corresponds to a terrace, a kink, and an edge or corner atom (Figure 2a), respectively. On {100} facets, a CN = 8 and ≤ 7 indicates a terrace and an edge or corner atom (Figure 2b), respectively. We calculated the ratio of low-coordination surface atoms (CN < 9 and CN < 8 for {111} and {100} facets, respectively) to the entire exposed surface atoms (CN ≤ 9 and CN ≤ 8 for {111} and {100} facets, respectively). We compared the ratios obtained from our

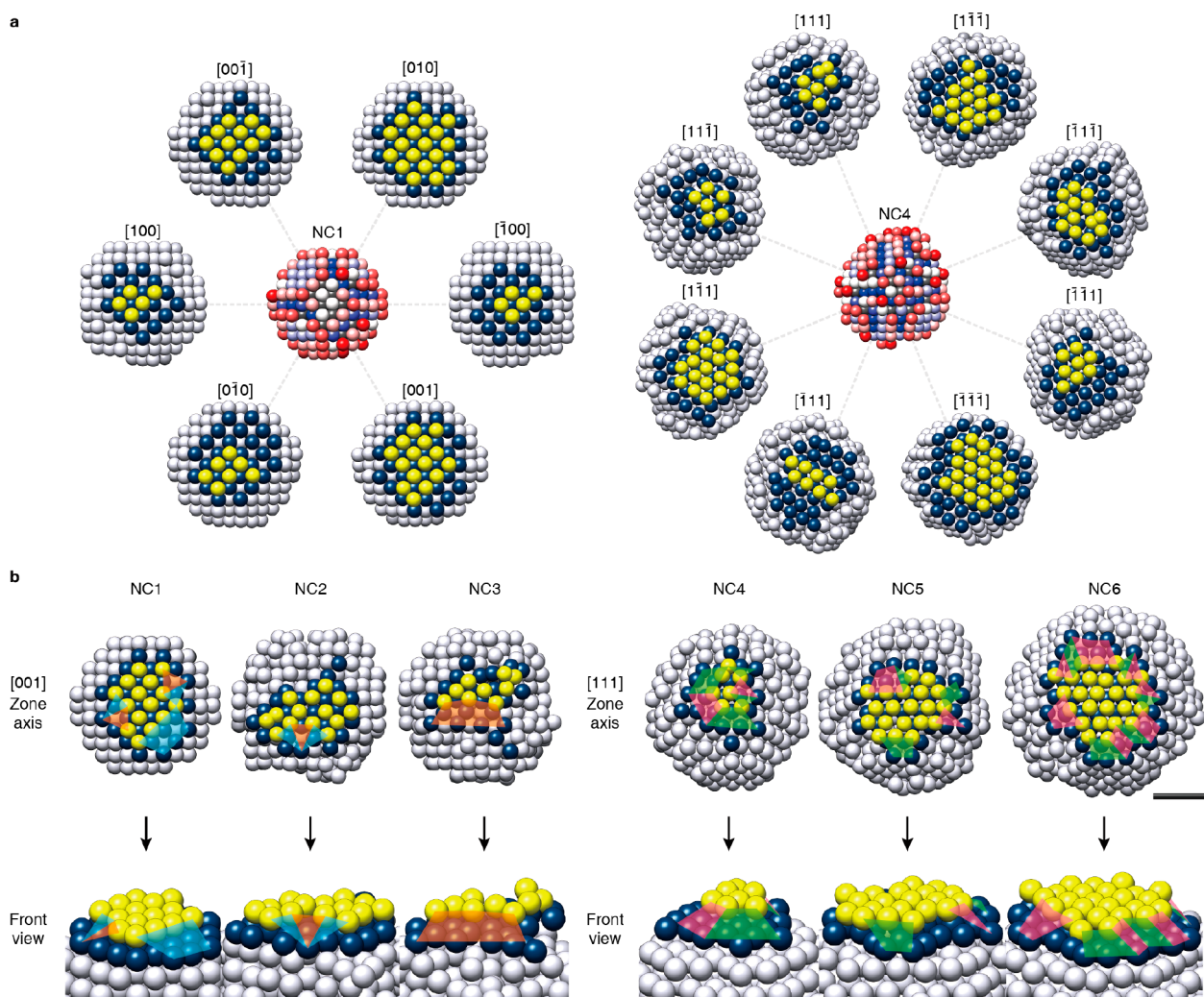


Figure 3. Complex and unique surface structures of the synthesized Pt nanocrystals enclosed by irregularly shaped islands. (a) Visualized surface structures of the synthesized Pt nanocrystals. Six individual $\{100\}$ facets of NC1 and eight individual $\{111\}$ facets of NC4 are presented. The outermost surface layers and the lower layers in each facet are visualized with yellow and blue colors, respectively. (b) A part of surface structures on six synthesized Pt nanocrystals for specific low-index facets and its front view. Irregular structures of islands cause various types of high-index facets (blue, (S)- $[2(100) \times (111)]$; orange, (S)- $[2(100) \times (110)]$; green, (S)- $[2(111) \times (111)]$; pink, (S)- $[2(111) \times (100)]$). Scale bars, 1 nm.

experimentally derived structures with various sized fcc model structures, such as cuboctahedron, truncated octahedron, octahedron, and cube (Figure 2c,d, Figures S6–11, and see Methods in Supporting Information). The ratios for fcc model structures consistently decrease as size increases. Among the four different types of morphologies investigated, the ratios for cuboctahedral and truncated octahedral models are generally higher than ones from other morphologies. Interestingly, the ratios of the synthesized Pt nanocrystals are greater than the ratios of all fcc model structures. In addition, the fractions of atoms at the edge, corner, and kink sites are more dominant than terrace atoms (Figure 2e,f and Figure S12). These findings indicate that our synthesized Pt nanocrystals contain a relatively smaller portion of terrace atoms, which is consistent with the observed increase in atoms with CN = 10–11 (Figure S5). Therefore, the surface atomic structures of small Pt nanocrystals are composed of reduced terrace atoms along with a significant presence of steps.

We defined the surface occupancy as the number of occupied sites in the outermost surface layer divided by the number of available atomic sites, given by the atomic arrangement of the

below layer (Figure S13). A surface occupancy of one means that atoms with a CN = 10–11 are absent on crystal surfaces. With a surface occupancy lower than one, atoms with CN = 10–11 appear (Figure S13). We calculated surface occupancies of the synthesized Pt nanocrystal structures for eight $\{111\}$ and six $\{100\}$ individual facets (Figures S14–19) and averaged $\{111\}$ and $\{100\}$ (Figure 2g,h), respectively. Averaged surface occupancies for $\{111\}$ and $\{100\}$ facets in all synthesized Pt nanocrystal structures are about 0.5, as shown in Figure 2g,h. This indicates that most surface structures of Pt nanocrystals are enclosed by islands of atoms with a considerable amount of steps present (Figure S13). Moreover, uneven surface occupancies observed in individual facets imply that the islands have nonuniform structures (Figure S20). The ratio of low-coordination surface atoms and the surface occupancies of low-index facets suggest that the surfaces of these NCs are predominantly surrounded by irregularly shaped islands with abundant steps.

The complex and heterogeneous surface structures can be visualized, as shown in Figure 3. On individual low-index facets, the outermost surface atoms and the lower layer are colored in

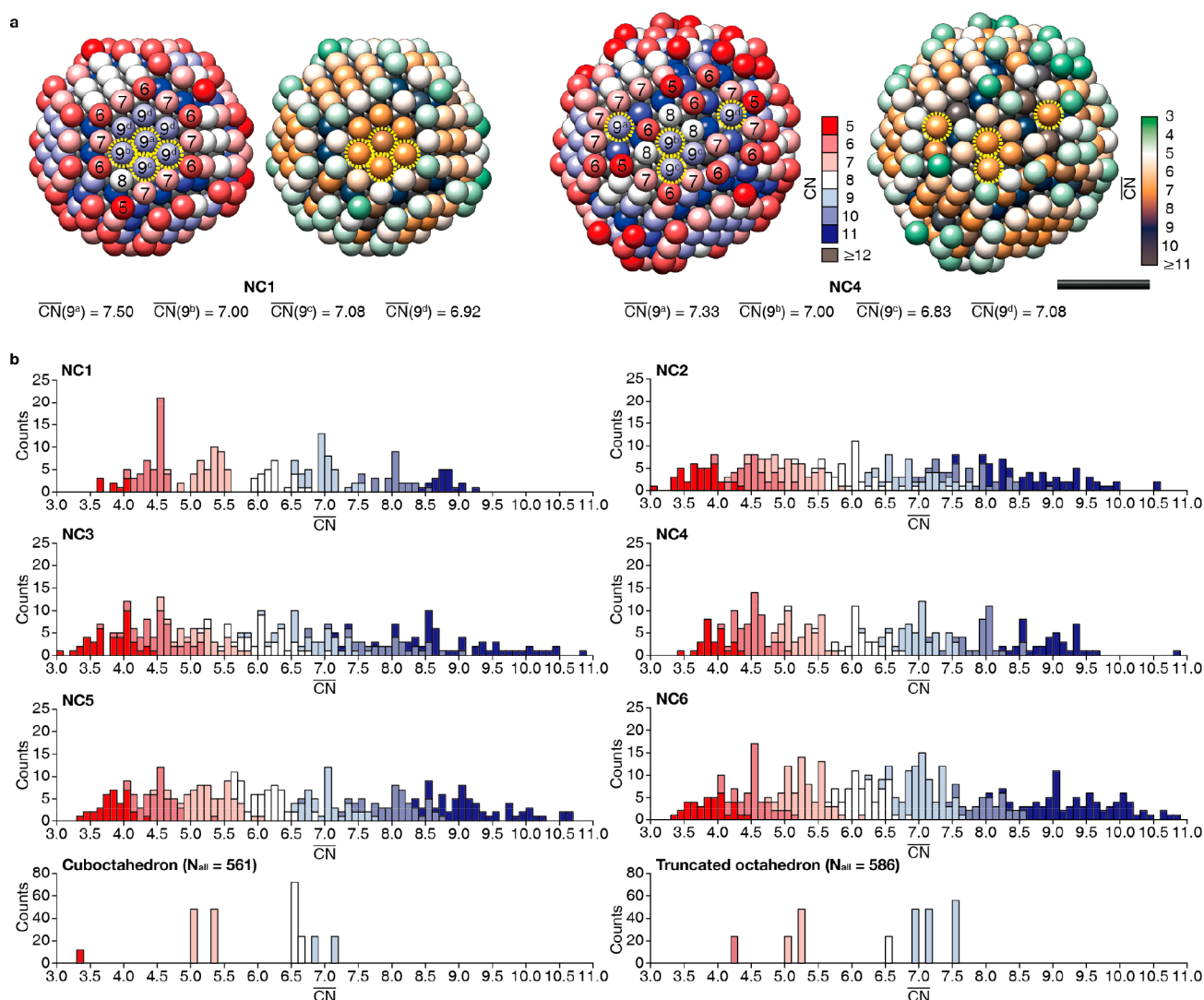


Figure 4. Complex surface structures of synthesized Pt nanocrystals along with a wide range of \overline{CN} s. (a) 3D maps of CN (left) with a color gradient from red to blue and \overline{CN} (right) with a color gradient from green to dark gray for NC1 and NC4. Surface atoms with the same CN = 9, surrounded by different surface geometries, show various \overline{CN} values. Scale bar, 1 nm. (b) Histograms for \overline{CN} of surface atoms with a color gradient given by their corresponding CN.

yellow and blue, respectively (Figure 3a). Islands on different exposed surfaces have distinct shapes and sizes with a reduced number of terrace atoms (Figure 3a). In addition, the irregular structures of the islands expose various high-index facets (Figure 3a,b). Four representative types of high-index facets based on $\{111\}$ and $\{100\}$ facets, (S)- $[2(100) \times (111)]$, (S)- $[2(100) \times (110)]$, (S)- $[2(111) \times (111)]$, and (S)- $[2(111) \times (100)]$, are depicted in Figure 3b, and there are more of the exposed high-index facets such as (S)- $[3(h_s k_s l_s) \times (h_s k_s l_s)]$ and (S)- $[4(h_s k_s l_s) \times (h_s k_s l_s)]$ (Figure S21).¹

The lower CN of surface atoms is directly related to a tendency to form bonds with external species, explaining their catalytic reactivity.^{41–44} However, it is not straightforward to predict catalytic performance based on CN, since surface atoms with the same CN are often surrounded by different surface geometries and show dissimilar adsorption properties.^{42,43} A more appropriate descriptor for adsorption properties and catalytic activities is the generalized coordination number (\overline{CN}), an extension of CN that considers CNs of the first nearest neighbor atoms enclosing a surface atom of interest.^{27,45,46} \overline{CN}

of an atom i surrounded by the first nearest neighbor atoms of j is defined by

$$\overline{CN}_i = \sum_{k=1}^j \frac{CN(k)}{CN_{\max}}, \quad (1)$$

where CN_{\max} and $CN(k)$ denote the maximum CN of the first nearest neighbor atoms and CN of each first nearest neighbor atom, respectively. According to eq 1, \overline{CN} varies depending on the CNs of the first nearest neighbor atoms. It is found that surface atoms of the Pt nanocrystals with the same CN show different \overline{CN} s, as shown in the comparison of 3D maps of CN and \overline{CN} in Figure 4a. For example, surface atoms with the same CN ($CN = 9$) indicated by dashed yellow circles in Figure 4a have \overline{CN} s in a range from 6.92 to 7.50 and from 6.83 to 7.33 for NC1 and NC4, respectively (Figure S22). This implies that they are surrounded by different geometries, and this tendency is consistently observed in all surface atoms. Histograms of the \overline{CN} s for surface atoms with a given CN are shown in Figure 4b. Histograms are colored by red to blue, which corresponds to CNs of 5–11. The distribution of values in the histograms for

the synthesized Pt nanocrystals is generally delocalized in a wide range in contrast to the expected narrow distribution of $\overline{\text{CN}}$ s for fcc model structures with regular surface geometry (Figure 4b, bottom row), confirming that the surface structures of synthesized Pt nanocrystals incorporate diverse local geometries. Summarizing findings based on 3D maps of CN and $\overline{\text{CN}}$, the synthesized Pt nanocrystals have complex surface structures, enclosed by islands of atoms with nonuniform structures, which have distinct characteristics such as a high ratio of low-coordination surface atoms, reduced domain size of low-index facets, and various types of exposed high-index facets.

Our efforts to quantitatively characterize the surface structures of the Pt nanocrystals in terms of CN and $\overline{\text{CN}}$ of all exposed surface atoms can aid in predicting the catalytic activities of heterogeneous catalysts. Small Pt nanocrystals are commonly used as fuel cell catalysts,^{45–52} specifically in the ORR and CO electro-oxidation. We estimated the catalytic activities of the synthesized Pt nanocrystals in acidic media by using previously reported scaling relations between $\overline{\text{CN}}$ and catalytic properties (Figure 5 and see Methods in Supporting

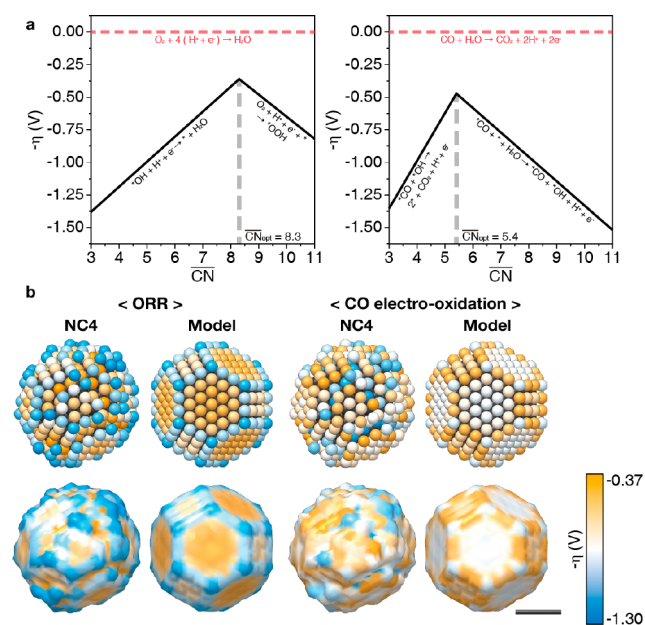


Figure 5. Prediction of local catalytic activities in ORR and CO electro-oxidation. (a) Theoretically estimated relationship between $\overline{\text{CN}}$ and overpotential for ORR and CO electro-oxidation of Pt. Optimal $\overline{\text{CN}}$ for ORR and CO electro-oxidation is 8.3 and 5.4, respectively. (b) 3D color maps of overpotential for ORR and CO electro-oxidation overlaid on atom position and surface contour. A scale of overpotential (η) is represented by a color gradient from orange to blue.

Information).^{45,46} Theoretically calculated volcano plots between overpotential (η) and $\overline{\text{CN}}$ were adopted from the previous report and shown in Figure 5a.^{45,46} Overpotential is necessary to overcome the kinetic barrier of the electrochemical reaction. A reduced overpotential means a low kinetic barrier, which results in an enhanced reaction rate.^{45–47} The estimated optimal $\overline{\text{CN}}$ with the least overpotential for ORR and CO electro-oxidation is 8.3 and 5.4, respectively^{45,46} (Figure 5a). As the $\overline{\text{CN}}$ moves away from the optimal value, the corresponding overpotential increases, which indicates lowered catalytic activity. 3D atom coordinates and surface contours are shown by a color gradient from orange to blue, corresponding to a low

to high overpotential (Figure 5b). For the synthesized Pt nanocrystals, their distinctive structural characteristics influence the distribution of local catalytic activities. In the ORR map, surface atoms with an orange color are mainly located in {111} terraces and bottom of steps, while a high ratio of low-coordination surface atoms leads to areas of high overpotential (blue color) at edges and corners. Meanwhile, for CO electro-oxidation, surface atoms with an orange color are mainly located at edges and {100} terraces, while surface atoms with a blue color appear in the bottom of steps and several protruded corners. These geometric features are consistent with the previous experimental results, demonstrating that different morphologies of catalysts lead to different catalytic activities.^{48–52} Compared to fcc model structures, the reduced size of {111} and {100} facets of the synthesized Pt nanocrystals results in a lowering of $\overline{\text{CN}}$. The reduced $\overline{\text{CN}}$ causes the catalytic activity of terrace atoms to decrease and increase for ORR and CO electro-oxidation, respectively (Figures S23 and S24). At the same time, the reduction of terraces causes exposure of surface atoms located at the bottom of steps (CN = 10–11) with a high $\overline{\text{CN}}$, showing high and low catalytic activities indicated by the orange and blue colors in the ORR and CO electro-oxidation map, respectively. Consequently, the complex surface structures of the synthesized Pt nanocrystals give rise to a wide range of $\overline{\text{CN}}$ accompanied by exposure of diverse local surface geometries that have intrinsic catalytic activities toward different reactions. This explains why sub-3 nm Pt nanocrystals are effective in many different catalytic reactions.

The analysis for atomic CN and $\overline{\text{CN}}$ for sub-3 nm Pt nanocrystals is based on atomic resolution 3D reconstruction of individual nanocrystals dispersed in solution.⁴⁰ The surface chemistry we understand based on this model system may have disparity with Pt heterogeneous catalysts used in diverse catalytic systems. Nevertheless, an attempt to correlate local structures with catalytic activities of the entire surface-exposed constituent atoms suggests a new quantitative method that delivers unprecedented physical perspective underlying the activities of heterogeneous catalysis. Extending the use of “one-particle reconstruction” to various catalytic systems, such as large Pt nanocrystals and nanocrystals with different compositions, along with its combination with quantitative analysis for atomic CN and $\overline{\text{CN}}$ would advance itself to an efficient platform for studying heterogeneous catalysis. Furthermore, the characteristic surface structures of the synthesized Pt nanocrystals, enclosed by islands of atoms with irregular structures, reveal a structural arrangement that can explain general behaviors of heterogeneous Pt catalysts with similar size. There are already several reports verifying that supported heterogeneous Pt nanocrystals are not truncated by perfectly flat surfaces.^{34,35,53–57} We also characterized commercial Pt/C with aberration-corrected HR-TEM (Figure S25 and see Methods in Supporting Information) and confirmed that surface structures of sub-3 nm sized Pt nanocrystals on carbon support are indeed enclosed by irregularly shaped islands of atoms.

In conclusion, we constructed 3D maps of atomic CN, $\overline{\text{CN}}$, and catalytic activity for sub-3 nm sized synthesized Pt nanocrystals, which can be extensively exploited to understand surface geometric effects in catalytic activities of heterogeneous catalysts. Our results reveal that the surface structures are enclosed by islands of atoms with nonuniform structures, accompanied by a high ratio of low-coordination surface atoms, small domain size of low-index facets, and various types of

exposed high-index facets. These distinctive surface characteristics of the synthesized Pt nanocrystals explain their unique activities observed in different catalytic reactions. In addition, our findings can be used to reduce disparities between catalytic activity estimated in the theoretical calculation based on structure models and their measured experimental activity.

■ ASSOCIATED CONTENT

SI Supporting Information

The Supporting Information is available free of charge at <https://pubs.acs.org/doi/10.1021/acs.nanolett.0c04873>.

Additional experimental methods (PDF)

■ AUTHOR INFORMATION

Corresponding Authors

Peter Ercius – National Center for Electron Microscopy, Molecular Foundry, Lawrence Berkeley National Laboratory, Berkeley, California 94720, United States; orcid.org/0000-0002-6762-9976; Email: percious@lbl.gov

Hans Elmlund – Department of Biochemistry and Molecular Biology, Biomedicine Discovery Institute, Monash University, Clayton, Victoria 3800, Australia; ARC Centre of Excellence for Advanced Molecular Imaging, Clayton, Victoria 3800, Australia; orcid.org/0000-0002-6992-0601; Email: hans.elmlund@monash.edu

Jungwon Park – Center for Nanoparticle Research, Institute for Basic Science (IBS), Seoul 08826, Republic of Korea; School of Chemical and Biological Engineering, and Institute of Chemical Processes, Seoul National University, Seoul 08826, Republic of Korea; orcid.org/0000-0003-2927-4331; Email: jungwonpark@snu.ac.kr

Authors

Sungin Kim – Center for Nanoparticle Research, Institute for Basic Science (IBS), Seoul 08826, Republic of Korea; School of Chemical and Biological Engineering, and Institute of Chemical Processes, Seoul National University, Seoul 08826, Republic of Korea; orcid.org/0000-0001-9107-0781

Jimin Kwag – School of Chemical and Biological Engineering, and Institute of Chemical Processes, Seoul National University, Seoul 08826, Republic of Korea

Chiara Machello – Department of Biochemistry and Molecular Biology, Biomedicine Discovery Institute, Monash University, Clayton, Victoria 3800, Australia; ARC Centre of Excellence for Advanced Molecular Imaging, Clayton, Victoria 3800, Australia

Sungsu Kang – Center for Nanoparticle Research, Institute for Basic Science (IBS), Seoul 08826, Republic of Korea; School of Chemical and Biological Engineering, and Institute of Chemical Processes, Seoul National University, Seoul 08826, Republic of Korea

Junyoung Heo – Center for Nanoparticle Research, Institute for Basic Science (IBS), Seoul 08826, Republic of Korea; School of Chemical and Biological Engineering, and Institute of Chemical Processes, Seoul National University, Seoul 08826, Republic of Korea

Cyril F. Reboul – Department of Biochemistry and Molecular Biology, Biomedicine Discovery Institute, Monash University, Clayton, Victoria 3800, Australia; ARC Centre of Excellence for Advanced Molecular Imaging, Clayton, Victoria 3800, Australia

Dohun Kang – School of Chemical and Biological Engineering, and Institute of Chemical Processes, Seoul National University, Seoul 08826, Republic of Korea

Seulki Kang – Department of Chemistry and Nanoscience, Ewha Womans University, Seoul 03760, Republic of Korea

Sangdeok Shim – Department of Chemistry, Sunchon National University, Suncheon 57922, Republic of Korea; orcid.org/0000-0001-5887-565X

So-Jung Park – Department of Chemistry and Nanoscience, Ewha Womans University, Seoul 03760, Republic of Korea; orcid.org/0000-0002-6364-3754

Byung Hyo Kim – Center for Nanoparticle Research, Institute for Basic Science (IBS), Seoul 08826, Republic of Korea; School of Chemical and Biological Engineering, and Institute of Chemical Processes, Seoul National University, Seoul 08826, Republic of Korea; Department of Organic Materials and Fiber Engineering, Soongsil University, Seoul 06978, Republic of Korea

Taeghwan Hyeon – Center for Nanoparticle Research, Institute for Basic Science (IBS), Seoul 08826, Republic of Korea; School of Chemical and Biological Engineering, and Institute of Chemical Processes, Seoul National University, Seoul 08826, Republic of Korea; orcid.org/0000-0001-5959-6257

Complete contact information is available at: <https://pubs.acs.org/doi/10.1021/acs.nanolett.0c04873>

Author Contributions

S.K., C.M., J.H., H.E., and J.P. planned the research. S.K., C.M., J.H., C.R., D.K., B.H.K., P.E., T.H., H.E., and J.P. acquired the 3D atomic structures. S.K., J.K., and J.P. analyzed and interpreted the results. S.K. and S.K. acquired HR-TEM images of commercial Pt/C catalysts. S.K., J.K., J.H., S.K., S.S., S.-J.P., B.H.K., T.H., P.E., H.E., and J.P. wrote the manuscript. P.E., H.E., and J.P. supervised the research. All authors contributed to the discussion of the results. All authors have given approval to the final version of the manuscript.

Notes

The authors declare no competing financial interest.

■ ACKNOWLEDGMENTS

J.P. and T.H. acknowledge the Institute for Basic Science (IBS-R006-D1). J.P. and S.-J.P. acknowledge the National Research Foundation of Korea (NRF) grant funded by the Korea government (MSIT) (NRF-2017R1A5A1015365). J.P. acknowledges the National Research Foundation of Korea (NRF) grant funded by the Korea government (MSIT) (NRF-2019M3E6A1064877 and NRF-2020R1A2C2101871). S.K., S.K., J.H., and J.P. acknowledge support by Samsung Science and Technology Foundation under project no. SSTF-BA1802-08 for sample preparation and algorithm development. Theoretical computation was supported by the National Supercomputing Center with supercomputing resources including technical support (KSC-2019-CRE-0119). H.E. acknowledges the Australian Research Council (ARC) grant DP170101850 and the National Health and Medical Research Council, Australia, grant APP1125909. C.F.R. acknowledges Early Career Fellowship (APP1122769). The work was supported by the Molecular Foundry, Lawrence Berkeley National Laboratory, which is supported by the U.S. Department of Energy under contract no. DE-AC02-05CH11231

■ REFERENCES

- (1) Somorjai, G. A.; Li, Y. *Introduction to surface chemistry and catalysis*; John Wiley & Sons, 2010.
- (2) Lee, I.; Delbecq, F.; Morales, R.; Albitzer, M. A.; Zaera, F. Tuning selectivity in catalysis by controlling particle shape. *Nat. Mater.* **2009**, *8* (2), 132–138.
- (3) Kang, Y. J.; Qi, L.; Li, M.; Diaz, R. E.; Su, D.; Adzic, R. R.; Stach, E.; Li, J.; Murray, C. B. Highly Active Pt₃Pb and Core-Shell Pt₃Pb-Pt Electrocatalysts for Formic Acid Oxidation. *ACS Nano* **2012**, *6* (3), 2818–2825.
- (4) Baldi, A.; Narayan, T. C.; Koh, A. L.; Dionne, J. A. In situ detection of hydrogen-induced phase transitions in individual palladium nanocrystals. *Nat. Mater.* **2014**, *13* (12), 1143–1148.
- (5) Manthiram, K.; Beberwyck, B. J.; Alivisatos, A. P. Enhanced Electrochemical Methanation of Carbon Dioxide with a Dispersible Nanoscale Copper Catalyst. *J. Am. Chem. Soc.* **2014**, *136* (38), 13319–13325.
- (6) Cao, S. W.; Tao, F.; Tang, Y.; Li, Y. T.; Yu, J. G. Size- and shape-dependent catalytic performances of oxidation and reduction reactions on nanocatalysts. *Chem. Soc. Rev.* **2016**, *45* (17), 4747–4765.
- (7) Narayan, T. C.; Hayee, F.; Baldi, A.; Koh, A. L.; Sinclair, R.; Dionne, J. A. Direct visualization of hydrogen absorption dynamics in individual palladium nanoparticles. *Nat. Commun.* **2017**, *8*, 14020.
- (8) Luo, B. B.; Smith, J. W.; Ou, Z. H.; Chen, Q. Quantifying the Self-Assembly Behavior of Anisotropic Nanoparticles Using Liquid-Phase Transmission Electron Microscopy. *Acc. Chem. Res.* **2017**, *50* (5), 1125–1133.
- (9) Ou, Z. H.; Song, X. H.; Huang, W.; Jiang, X.; Qu, S. B.; Wang, Q. Y.; Braun, P. V.; Moore, J. S.; Li, X. L.; Chen, Q. Colloidal Metal-Organic Framework Hexapods Prepared from Postsynthesis Etching with Enhanced Catalytic Activity and Rollable Packing. *ACS Appl. Mater. Interfaces* **2018**, *10* (48), 40990–40995.
- (10) Hayee, F.; Narayan, T. C.; Nadkarni, N.; Baldi, A.; Koh, A. L.; Bazant, M. Z.; Sinclair, R.; Dionne, J. A. In-situ visualization of solute-driven phase coexistence within individual nanorods. *Nat. Commun.* **2018**, *9*, 1775.
- (11) Kim, A.; Zhou, S.; Yao, L. H.; Ni, S.; Luo, B. B.; Sing, C. E.; Chen, Q. Tip-Patched Nanoprisms from Formation of Ligand Islands. *J. Am. Chem. Soc.* **2019**, *141* (30), 11796–11800.
- (12) Lee, J. D.; Jishkariani, D.; Zhao, Y. R.; Najmr, S.; Rosen, D.; Kikkawa, J. M.; Stach, E. A.; Murray, C. B. Tuning the Electrocatalytic Oxygen Reduction Reaction Activity of Pt-Co Nanocrystals by Cobalt Concentration with Atomic-Scale Understanding. *ACS Appl. Mater. Interfaces* **2019**, *11* (30), 26789–26797.
- (13) Corbin, N.; Zeng, J.; Williams, K.; Manthiram, K. Heterogeneous molecular catalysts for electrocatalytic CO₂ reduction. *Nano Res.* **2019**, *12* (9), 2093–2125.
- (14) Park, J.; Jin, K.; Sahasrabudhe, A.; Chiang, P. H.; Maalouf, J. H.; Koehler, F.; Rosenfeld, D.; Rao, S.; Tanaka, T.; Khudiyev, T.; Schiffer, Z. J.; Fink, Y.; Yizhar, O.; Manthiram, K.; Anikeeva, P. In situ electrochemical generation of nitric oxide for neuronal modulation. *Nat. Nanotechnol.* **2020**, *15* (8), 690–697.
- (15) Bratlie, K. M.; Lee, H.; Komvopoulos, K.; Yang, P. D.; Somorjai, G. A. Platinum nanoparticle shape effects on benzene hydrogenation selectivity. *Nano Lett.* **2007**, *7* (10), 3097–3101.
- (16) Huang, X. Q.; Zhao, Z. P.; Cao, L.; Chen, Y.; Zhu, E. B.; Lin, Z. Y.; Li, M. F.; Yan, A. M.; Zettl, A.; Wang, Y. M.; Duan, X. F.; Mueller, T.; Huang, Y. High-performance transition metal-doped Pt₃Ni octahedra for oxygen reduction reaction. *Science* **2015**, *348* (6240), 1230–1234.
- (17) Stamenkovic, V.; Markovic, N. M.; Ross, P. N. Structure-relationships in electrocatalysis: oxygen reduction and hydrogen oxidation reactions on Pt(111) and Pt(100) in solutions containing chloride ions. *J. Electroanal. Chem.* **2001**, *500* (1–2), 44–51.
- (18) Kang, Y. J.; Murray, C. B. Synthesis and Electrocatalytic Properties of Cubic Mn-Pt Nanocrystals (Nanocubes). *J. Am. Chem. Soc.* **2010**, *132* (22), 7568–7569.
- (19) Kim, S. K.; Kim, C.; Lee, J. H.; Kim, J.; Lee, H.; Moon, S. H. Performance of shape-controlled Pd nanoparticles in the selective hydrogenation of acetylene. *J. Catal.* **2013**, *306*, 146–154.
- (20) Yoon, D.; Seo, B.; Lee, J.; Nam, K. S.; Kim, B.; Park, S.; Baik, H.; Joo, S. H.; Lee, K. Facet-controlled hollow Rh₂S₃ hexagonal nanoprisms as highly active and structurally robust catalysts toward hydrogen evolution reaction. *Energy Environ. Sci.* **2016**, *9* (3), 850–856.
- (21) Seo, B.; Baek, D. S.; Sa, Y. J.; Joo, S. H. Shape effects of nickel phosphide nanocrystals on hydrogen evolution reaction. *CrystEngComm* **2016**, *18* (32), 6083–6089.
- (22) Yin, Z. W.; Betzler, S. B.; Sheng, T.; Zhang, Q. B.; Peng, X. X.; Shangquan, J.; Bustillo, K. C.; Li, J. T.; Sun, S. G.; Zheng, H. M. Visualization of facet-dependent pseudo-photocatalytic behavior of TiO₂ nanorods for water splitting using In situ liquid cell TEM. *Nano Energy* **2019**, *62*, 507–512.
- (23) Gamler, J. T. L.; Shin, K.; Ashberry, H. M.; Chen, Y. F.; Bueno, S. L. A.; Tang, Y. W.; Henkelman, G.; Skrabalak, S. E. Intermetallic Pd₃Pb nanocubes with high selectivity for the 4-electron oxygen reduction reaction pathway. *Nanoscale* **2020**, *12* (4), 2532–2541.
- (24) Gan, L.; Heggen, M.; Cui, C. H.; Strasser, P. Thermal Facet Healing of Concave Octahedral Pt-Ni Nanoparticles Imaged in Situ at the Atomic Scale: Implications for the Rational Synthesis of Durable High-Performance ORR Electrocatalysts. *ACS Catal.* **2016**, *6* (2), 692–695.
- (25) Liao, H. G.; Zheng, H. M. Liquid Cell Transmission Electron Microscopy Study of Platinum Iron Nanocrystal Growth and Shape Evolution. *J. Am. Chem. Soc.* **2013**, *135* (13), 5038–5043.
- (26) Zheng, L. Y.; Zhao, L. X.; Zhao, S. H.; Zhang, X. W.; Bustillo, K. C.; Yao, Y.; Yi, X. F.; Zhu, M. G.; Li, W.; Zheng, H. M. A unique pathway of PtNi nanoparticle formation observed with liquid cell transmission electron microscopy. *Nanoscale* **2020**, *12* (3), 1414–1418.
- (27) Jorgensen, M.; Gronbeck, H. The Site-Assembly Determines Catalytic Activity of Nanoparticles. *Angew. Chem., Int. Ed.* **2018**, *57* (18), 5086–5089.
- (28) Yang, A.-C.; Choksi, T.; Streibel, V.; Aljama, H.; Wrasman, C. J.; Roling, L. T.; Goodman, E. D.; Thomas, D.; Bare, S. R.; Sánchez-Carrera, R. S.; Schafer, A.; Li, Y. J.; Abild-Pedersen, F.; Cargnello, M. Revealing the structure of a catalytic combustion active-site ensemble combining uniform nanocrystal catalysts and theory insights. *Proc. Natl. Acad. Sci. U. S. A.* **2020**, *117* (26), 14721–14729.
- (29) Joo, S. H.; Kwon, K.; You, D. J.; Pak, C.; Chang, H.; Kim, J. M. Preparation of high loading Pt nanoparticles on ordered mesoporous carbon with a controlled Pt size and its effects on oxygen reduction and methanol oxidation reactions. *Electrochim. Acta* **2009**, *54* (24), 5746–5753.
- (30) Arenz, M.; Mayrhofer, K. J. J.; Stamenkovic, V.; Blizanac, B. B.; Tomoyuki, T.; Ross, P. N.; Markovic, N. M. The effect of the particle size on the kinetics of CO electrooxidation on high surface area Pt catalysts. *J. Am. Chem. Soc.* **2005**, *127* (18), 6819–6829.
- (31) Shao, M.; Peles, A.; Shoemaker, K. Electrocatalysis on platinum nanoparticles: particle size effect on oxygen reduction reaction activity. *Nano Lett.* **2011**, *11* (9), 3714–3719.
- (32) Reske, R.; Mistry, H.; Behafarid, F.; Roldan Cuenya, B.; Strasser, P. Particle size effects in the catalytic electroreduction of CO₂ on Cu nanoparticles. *J. Am. Chem. Soc.* **2014**, *136* (19), 6978–6986.
- (33) Willis, J. J.; Gallo, A.; Sokaras, D.; Aljama, H.; Nowak, S. H.; Goodman, E. D.; Wu, L. H.; Tassone, C. J.; Jaramillo, T. F.; Abild-Pedersen, F.; Cargnello, M. Systematic Structure Property Relationship Studies in Palladium Catalyzed Methane Complete Combustion. *ACS Catal.* **2017**, *7* (11), 7810–7821.
- (34) Gontard, L. C.; Chang, L. Y.; Hetherington, C. J. D.; Kirkland, A. I.; Ozkaya, D.; Dunin-Borkowski, R. E. Aberration-corrected imaging of active sites on industrial catalyst nanoparticles. *Angew. Chem., Int. Ed.* **2007**, *46* (20), 3683–3685.
- (35) Chang, L. Y.; Barnard, A. S.; Gontard, L. C.; Dunin-Borkowski, R. E. Resolving the Structure of Active Sites on Platinum Catalytic Nanoparticles. *Nano Lett.* **2010**, *10* (8), 3073–3076.
- (36) Chen, C. C.; Zhu, C.; White, E. R.; Chiu, C. Y.; Scott, M. C.; Regan, B. C.; Marks, L. D.; Huang, Y.; Miao, J. W. Three-dimensional imaging of dislocations in a nanoparticle at atomic resolution. *Nature* **2013**, *496* (7443), 74–77.

- (37) Yang, Y.; Chen, C. C.; Scott, M. C.; Ophus, C.; Xu, R.; Pryor, A.; Wu, L.; Sun, F.; Theis, W.; Zhou, J. H.; Eisenbach, M.; Kent, P. R. C.; Sabirianov, R. F.; Zeng, H.; Ercius, P.; Miao, J. W. Deciphering chemical order/disorder and material properties at the single-atom level. *Nature* **2017**, *542* (7639), 75–79.
- (38) Pryor, A.; Yang, Y.; Rana, A.; Gallagher-Jones, M.; Zhou, J. H.; Lo, Y. H.; Melinte, G.; Chiu, W.; Rodriguez, J. A.; Miao, J. W. GENFIRE: A generalized Fourier iterative reconstruction algorithm for high-resolution 3D imaging. *Sci. Rep.* **2017**, *7*, 10409.
- (39) Zhou, J. H.; Yang, Y.; Yang, Y.; Kim, D. S.; Yuan, A.; Tian, X. Z.; Ophus, C.; Sun, F.; Schmid, A. K.; Nathanson, M.; Heinz, H.; An, Q.; Zeng, H.; Ercius, P.; Miao, J. W. Observing crystal nucleation in four dimensions using atomic electron tomography. *Nature* **2019**, *570* (7762), 500–503.
- (40) Kim, B. H.; Heo, J.; Kim, S.; Reboul, C. F.; Chun, H.; Kang, D.; Bae, H.; Hyun, H.; Lim, J.; Lee, H.; Han, B.; Hyeon, T.; Alivisatos, A. P.; Ercius, P.; Elmlund, H.; Park, J. Critical differences in 3D atomic structure of individual ligand-protected nanocrystals in solution. *Science* **2020**, *368* (6486), 60–67.
- (41) Jiang, T.; Mowbray, D. J.; Dobrin, S.; Falsig, H.; Hvolbaek, B.; Bligaard, T.; Norskov, J. K. Trends in CO Oxidation Rates for Metal Nanoparticles and Close-Packed, Stepped, and Kinked Surfaces. *J. Phys. Chem. C* **2009**, *113* (24), 10548–10553.
- (42) Calle-Vallejo, F.; Loffreda, D.; Koper, M. T. M.; Sautet, P. Introducing structural sensitivity into adsorption-energy scaling relations by means of coordination numbers. *Nat. Chem.* **2015**, *7* (5), 403–410.
- (43) Roling, L. T.; Li, L.; Abild-Pedersen, F. Configurational Energies of Nanoparticles Based on Metal-Metal Coordination. *J. Phys. Chem. C* **2017**, *121* (41), 23002–23010.
- (44) Berwanger, J.; Polesya, S.; Mankovsky, S.; Ebert, H.; Giessibl, F. J. Atomically Resolved Chemical Reactivity of Small Fe Clusters. *Phys. Rev. Lett.* **2020**, *124* (9), 096001.
- (45) Calle-Vallejo, F.; Tymoczko, J.; Colic, V.; Vu, Q. H.; Pohl, M. D.; Morgenstern, K.; Loffreda, D.; Sautet, P.; Schuhmann, W.; Bandarenka, A. S. Finding optimal surface sites on heterogeneous catalysts by counting nearest neighbors. *Science* **2015**, *350* (6257), 185–189.
- (46) Calle-Vallejo, F.; Pohl, M. D.; Bandarenka, A. S. Quantitative Coordination-Activity Relations for the Design of Enhanced Pt Catalysts for CO Electro-oxidation. *ACS Catal.* **2017**, *7* (7), 4355–4359.
- (47) Norskov, J. K.; Rossmeisl, J.; Logadottir, A.; Lindqvist, L.; Kitchin, J. R.; Bligaard, T.; Jonsson, H. Origin of the overpotential for oxygen reduction at a fuel-cell cathode. *J. Phys. Chem. B* **2004**, *108* (46), 17886–17892.
- (48) Mayrhofer, K. J. J.; Blizanac, B. B.; Arenz, M.; Stamenkovic, V. R.; Ross, P. N.; Markovic, N. M. The impact of geometric and surface electronic properties of Pt-catalysts on the particle size effect in electrocatalysis. *J. Phys. Chem. B* **2005**, *109* (30), 14433–14440.
- (49) Stamenkovic, V. R.; Fowler, B.; Mun, B. S.; Wang, G. F.; Ross, P. N.; Lucas, C. A.; Markovic, N. M. Improved oxygen reduction activity on Pt₃Ni(111) via increased surface site availability. *Science* **2007**, *315* (5811), 493–497.
- (50) Liang, Y. C.; McLaughlin, D.; Csoklich, C.; Schneider, O.; Bandarenka, A. S. The nature of active centers catalyzing oxygen electro-reduction at platinum surfaces in alkaline media. *Energy Environ. Sci.* **2019**, *12* (1), 351–357.
- (51) McPherson, I. J.; Ash, P. A.; Jones, L.; Varambhia, A.; Jacobs, R. M. J.; Vincent, K. A. Electrochemical CO Oxidation at Platinum on Carbon Studied through Analysis of Anomalous in Situ IR Spectra. *J. Phys. Chem. C* **2017**, *121* (32), 17176–17187.
- (52) Su, M.; Dong, J.-C.; Le, J.-B.; Zhao, Y.; Yang, W.-M.; Yang, Z.-L.; Attard, G.; Liu, G.-K.; Cheng, J.; Wei, Y.-M.; Tian, Z.-Q.; Li, J.-F. In Situ Raman Study of CO Electrooxidation on Pt (hkl) Single-Crystal Surfaces in Acidic Solution. *Angew. Chem., Int. Ed.* **2020**, *59* (52), 23554–23558.
- (53) Barnard, A. S.; Chang, L. Y. Thermodynamic Cartography and Structure/Property Mapping of Commercial Platinum Catalysts. *ACS Catal.* **2011**, *1* (2), 76–81.
- (54) Van Aert, S.; Batenburg, K. J.; Rossell, M. D.; Erni, R.; Van Tendeloo, G. Three-dimensional atomic imaging of crystalline nanoparticles. *Nature* **2011**, *470* (7334), 374–377.
- (55) Jones, L.; MacArthur, K. E.; Fauske, V. T.; van Helvoort, A. T. J.; Nellist, P. D. Rapid Estimation of Catalyst Nanoparticle Morphology and Atomic-Coordination by High-Resolution Z-Contrast Electron Microscopy. *Nano Lett.* **2014**, *14* (11), 6336–6341.
- (56) Aarons, J.; Jones, L.; Varambhia, A.; MacArthur, K. E.; Ozkaya, D.; Sarwar, M.; Skylaris, C. K.; Nellist, P. D. Predicting the Oxygen-Binding Properties of Platinum Nanoparticle Ensembles by Combining High-Precision Electron Microscopy and Density Functional Theory. *Nano Lett.* **2017**, *17* (7), 4003–4012.
- (57) De Wael, A.; De Backer, A.; Jones, L.; Varambhia, A.; Nellist, P. D.; Van Aert, S. Measuring Dynamic Structural Changes of Nanoparticles at the Atomic Scale Using Scanning Transmission Electron Microscopy. *Phys. Rev. Lett.* **2020**, *124* (10), 106105.